



Hyperspectral reconstruction of spectrometer data for the JWST

Ralph ABI RIZK

This proposal is submitted in partial fulfillment of the requirements for the Bachelor of Engineering degree in Communication Engineering at Holy Spirit University of Kaslik (USEK) and for the Master degree in image and signal processing at Bordeaux University

20/08/2018

Acknowledgment

Working in the L2s laboratory was a great experience for my academic background. I was surrounded with talented and passionate researchers that gave me the motivation to move forward with my knowledge and spread positive vibes and great ambiance in the lab. During these six months, I was able to learn a lot about the image processing and optic physics and apply it in astrophysics domain. This internship has enriched my knowledge and taught me how to do a research, analyze it and apply it, and gave me the passion and the will to become a future researcher, and I wouldn't be able to achieve it without the help and the acknowledgment of other specialists.

First, I want to thank my supervisor Mr. Orioux François for being present at every stage of my internship. He taught me a lot of theoretical lessons, practical work and analyzing methods. His exigence and accuracy gave me the motivation to achieve my internship and taught me also how to push further my thoughts.

I would also want to thank my laboratory colleagues who set a nice and comfortable work ambiance and were always present to help and give advice specially the PHD student Hadj-Youssef Amine who gave me a lot of references and provided me with explanations.

Furthermore, I want to thank my Masters professor Mr. Giovannelli Jean-François for giving me the opportunity to embark in this project and always finding solutions to every encountered problem.

Finally, I want to thank the head chef of the telecommunication department at USEK University-Lebanon Mr. Yaacoub Charles for being my pedagogical instructor and for giving me opportunity to study abroad and make this internship possible.

Contents

1. Research unit	7
1.1. Paris-Sud university	7
1.2. CNRS	7
1.3. CentraleSupélec.....	8
1.4. Signal and system laboratory	8
1.5. Inverse Problem Group (GPI)	8
2. James Webb Space Telescope (JWST)	9
2.1. JWST optics	11
2.2. JWST instruments	11
2.3. Problematic.....	12
3. MRS modeling.....	14
3.1. Spatial convolution.....	14
3.2. Spectral division.....	15
3.3. Spatial division.....	16
3.4. Dithering.....	19
3.5. Diffraction gratings	19
3.5.1. Diffraction impulse response	19
3.5.2. Diffraction gratings output.....	21
3.5.3. Diffraction gratings length calculations.....	21
3.6. Detector	23
4. Simulation and results	24
4.1. Spatial convolution.....	24
4.2. Cube spatial and spectral slicing	25
4.3. Diffraction gratings	27
4.3.1. Diffraction gratings approximation.....	27
5. Reconstruction of the astrophysics cube	32
5.1. Least squares method	32
5.2. Ill-posed problem and regularization	32
5.3. Simulation and results	33
5.3.1. Transpose calculation.....	33
5.3.2. Calculate optimal μ	34

5.3.3.	Optimization algorithm.....	34
5.3.4.	Results.....	36
6.	Conclusion.....	40
7.	Perspectives	40
I.	Annex 1.....	41

Abstract

Inversion approaches are highly used in astrophysics since the received data is modified due to the instrument components and its passage through the channel. In this report, our main purpose is to reconstruct a 3D astrophysics map from a 2D image issued from the Medium Resolution Spectroscopy (MRS) of the MIRI instrument in James Webb Space Telescope. MRS is a very complex component that allows access into the specter of the received object, due to the diffraction gratings present in this instrument, and allow hyperspectral measures.

In order to recuperate the original cube and apply the inversion methods, we must first study the MRS components and determine the instrument responses that modify the observed object. During the acquisition, the 3D observed object represented by 2 spatial dimensions and one spectral dimension will be spatially affected by optic response of the telescope and spectrally by the response of the diffraction gratings. The particularity of these responses is that they change according to the wavelength value, which will introduce non-stationary responses to our acquisition process that will complicate the interpretation of the data. Approached methods are used to handle the non-stationary responses with a sum of stationary responses which will differ this work from the classic hyperspectral measures.

After the acquisition process, we will reconstruct the original cube by using inversion approaches. We will adopt in this work the least square method for the inversion due to the linearity of the system, and we will talk about the ill-posed problem that this method causes and how to regulate the problem.

Scientific Context

1. Research unit

My internship took place at the L2s laboratory from 19/03/2018 till 31/08/2018. L2s is a public laboratory and a research mixt unit of CentraleSupélec, CNRS (Centre National de la Recherche Scientifique) and Université Paris-Sud. More precisely, I was working on my internship at the GPI (Groupe de problème inverse) division. In this chapter we will present the different research unit related to L2s.

1.1. Paris-Sud university

Paris-Sud is a public university dedicated to high level research. It is represented by the president Sylvie Retailleau elected on may 30th 2016. Paris-Sud university was founded in December 1970 when the centers at Orsay, Châtenay-Malabry, Sceaux, Cachan and Kremlin-Bicêtre were merged. Since then, because of the proximity of Paris-Sud University to the Atomic Energy Institute (CEA) and the CNRS laboratories in Gif sur Yvette, many institutes and laboratories, as well as academic schools like Polytechnique, HEC, IHES, ENSTA and others also came to this area. As a result, the Vallée de Chevreuse has become one of the most important and well-known areas in Europe for scientific research. Paris-Sud University is made up of five Training and Research Units, still referred to as "faculties", three IUTs (University Institutes of Technology), and one School of Engineering, all located to the south of Paris. The University's head office is in Orsay, in Essonne. Because of its exceptional environment, Paris-Sud University is able to maintain a close relationship with leading research organizations like CNRS, Inserm, Inria, Inra and CEA, and with the French Grandes Ecoles such as Polytechnique, Supélec and HEC. Within Paris-Sud University there are over 80 internationally known laboratories; more than 30 technological platforms are open to industry and these publish more than 5,000 scientific publications every year.

1.2. CNRS

The National Center for Scientific Research, or CNRS, is a public organization under the responsibility of the French Ministry of Education and Research. It was founded in 1939 by the governmental decree and it contains 10 institutes in all the fields of knowledge and has laboratories throughout France where they and employ a large body of tenured researchers, engineers, and support staff. The CNRS aims to a lot of goals such as developing scientific information, supporting research training and contributing to promote and apply research results.

1.3. CentraleSupélec

CentraleSupélec is a public institution under ministerial charter, devoted to the sciences and engineering. This charter is shared between the Ministry of Higher Education, Research and Innovation, and the Ministry of Economy, Industry and Digital Technologies. CentraleSupélec was officially established on January 1st, 2015, bringing together two leading engineering schools in France; Ecole Centrale Paris and Supélec. The co-operation between the two *grandes écoles*, as they are known in the French system, had progressively been gaining momentum since 2009, with sustained alliance in three core areas: engineering education, executive education and research. The academic and research excellence is nestled in the cooperations with large national institutions such as the CNRS, CEA, INRIA, ISERM and ONERA.

1.4. Signal and system laboratory

L2s laboratory is a research unit directed by Sliviu-lulian NICULESCU. It welcomes every year a remarkable number of interns and visitors, plus, the laboratory is formed of CNRS researchers, instructors, PHD and post-PHD students. L2s contributes to the methodological and theoretical development of signal processing, systems, and electromagnetic systems by its numerous publications. This laboratory participates in many scientific activities such as conferences and workshops on a local, national and international term.

1.5. Inverse Problem Group (GPI)

My internship took place in the GPI group one of the components of the signal division, represented by Aurélie FRAYSSE.

GPI activities mainly concerns image reconstruction and restauration for many fields such as medical imaging, astrophysics and geophysics by treating many essential subjects such as deconvolution, data fusion, Fourier transform, source separation. The main purpose of the GPI work is to propose method such as regularized method and Bayesian approaches in order to resolve what it's called ill posed problem in image inversion.

Introduction

This internship concerns the reconstruction of 3D astrophysics image having 2 spatial dimensions and one spectral dimension. We will be working on data issued from the spectroscopy instrument in James Webb Space Telescope (JWST). Researchers are interested in spectroscopy because it reveals important physical and chemical properties of the light observed. These instruments will introduce special effects to the observed object while being analyzed. The goal is to identify the components of the instrument and use this model in the image reconstruction in order to obtain a hyperspectral resolution for the reconstructed data.

2. James Webb Space Telescope (JWST)

Named after James-E Webb, the JWST is developed in collaboration among NASA, European space agency (ESA) and Canadian space agency (CSA). The telescope was supposed to be launched late 2018 by the Ariane 5 rocket but the launching was delayed to 2021. This project cost around 8.8 billion dollars for 5.5 years of operation but its instruments have a life expectancy of 10 years.

JWST covers a wide range of wavelengths that observes the mid-infrared range, from $0.6 \mu\text{m}$ to $28 \mu\text{m}$. This range will allow the observation of many astrophysics aspects like the redshifted objects and it will also help understanding the stars and planet formation since they emit radiations in the infrared band that are way too distant for other telescopes to observe. The telescope is also placed at the L_2 Lagrange point at about 1,500,000 km away from the earth orbit. This distance will make any hardware update or reparation on the telescope quasi-impossible after the launching. The particularity of the L_2 Lagrange point is that the telescope will keep all the sun, earth and moon on the same side which will allow the use of only a single sunshield that can block the light coming from the three bodies. The sunshield is folded 12 times to fit the Ariane 5 rocket. Once launched, the sunshield will unfold making a surface of 21.197m x 14.162m.

The importance of the sunshield is to assure that telescope will maintain a temperature below -220 degrees. If not, the telescope itself will start emitting in the infrared range which will cause unclear observations of the desired infrared light, and sometimes completely outshine them.

Figure 1: A representation of the JWST telescope (JWST NASA documentation)

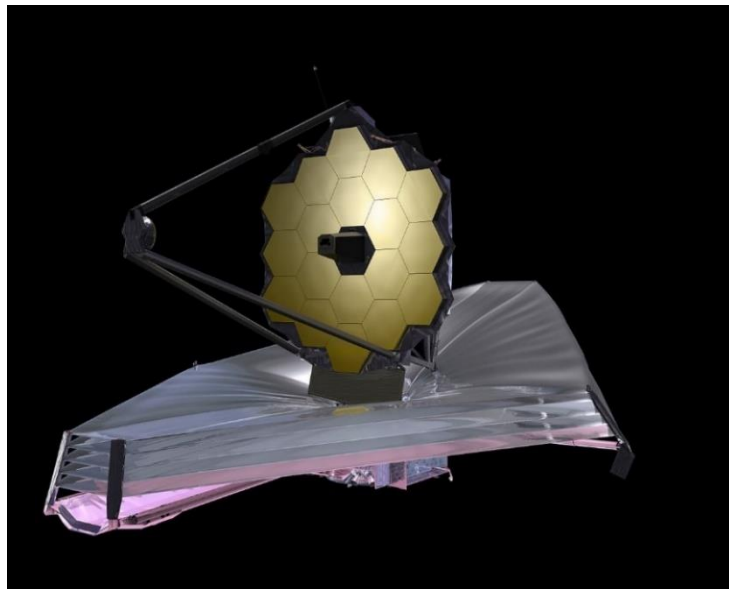
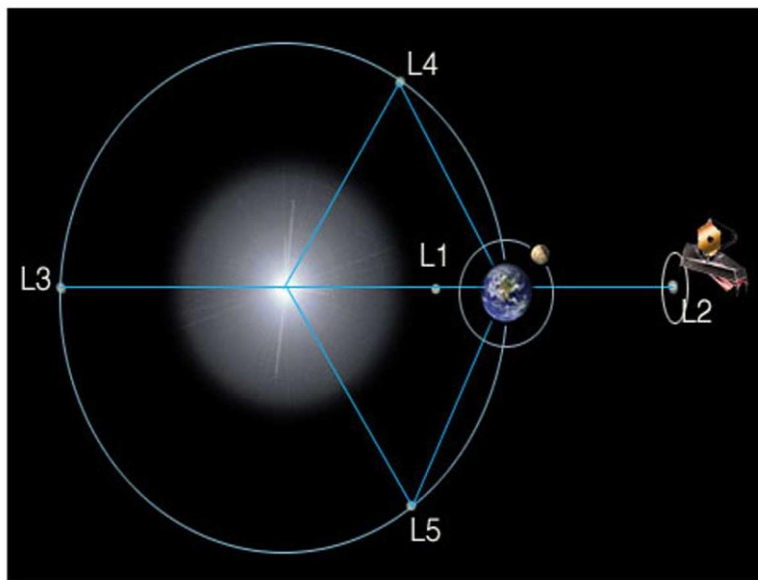


Figure 2: A representation of the Lagrange points in the space. Any Lagrange point keeps the same position between the earth and sun but the advantage of L2 is that it keeps all three bodies on the same side (Space.com science and astronomy)



2.1. JWST optics

JWST telescope contains a big mirror composed of 18 hexagonal segments folded before launching. Once launched in the space, these segments will be unfolded to form a mirror with a diameter of 6.5m. It is the biggest mirror ever to be sent to the space, it will permit to collect more photons which will increase the sensibility of the telescope and decrease the telescope limitation by the optical response of the mirror.

2.2. JWST instruments

The Integrated Science Instrument Module (ISIM) provides the electrical power resource, the structural stability and handles the cooling for the JWST. It contains four scientific instruments.

1. Near Infrared Camera (NIRCAM).

The NIRCAM is the JWST imager, covering from $0.6 \mu\text{m}$ through $5 \mu\text{m}$. It is occupied with a coronagraph that have a role of blocking the light of very bright objects and focuses on the nearby objects.

2. Near Infrared Spectrograph (NIRSpec)

NIRSpec covers the same range as NIRCAM but the difference between these two instruments is that NIRCAM works on imager and NIRSpec works on the spectroscopy.

3. Fine Guidance Sensor and Near Infrared Imager and Slitless Spectrograph (FGS/NIRISS)

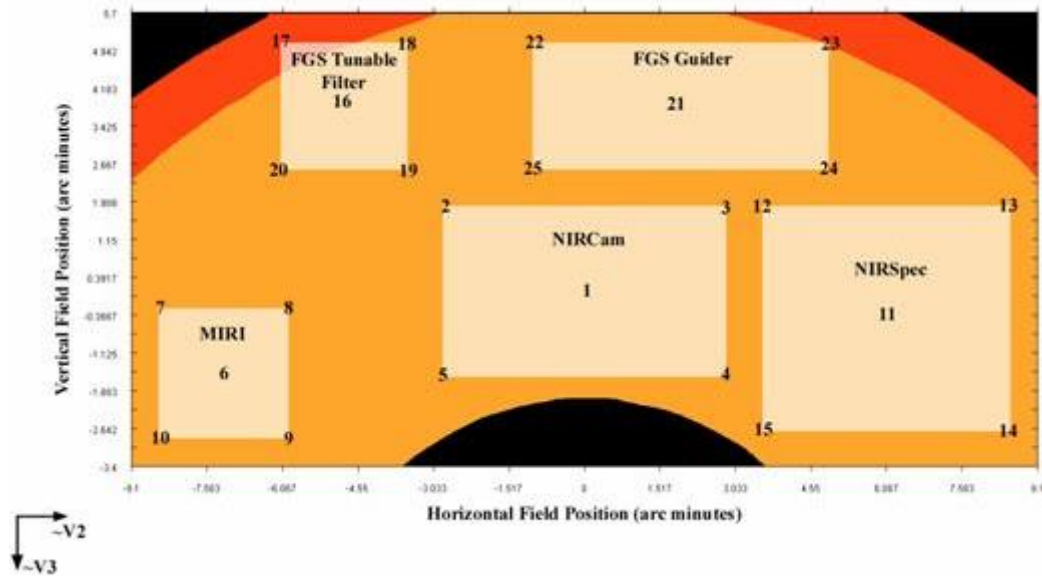
The FGS point the telescope which means that it stabilizes the line of sight of the observation. The NIRISS is composed of imaging and spectroscopy covering a range from $0.8 \mu\text{m}$ to $5 \mu\text{m}$.

4. Mid Infrared Instrument (MIRI)

The MIRI instrument covers a wavelength range from $4.85 \mu\text{m}$ to $28.45 \mu\text{m}$. It contains two main components, an imager (MIRIM) and a spectrograph. The main difference between these two components is that the imager has a high spatial resolution but a limited spectral resolution as for the spectrograph, it contains a high spectral resolution but a limited spatial resolution.

In this report, the MRS component of the MIRI instrument will be adopted. Since we are working on the hyperspectral measures, the spectrometer is used to separate the light of the observed 3D object. By doing that, astrophysicists can analyze the light to measure gas and analyze the chemical components of the stars and planets.

Figure 3: A representation of the spatial coordination in arc minutes of the instruments of JWST (James Webb Space Telescope documentation)



2.3. Problematic

We want to reconstruct a 3D infrared map for the astrophysicist to allow a better interpretation of the received data by using reconstruction methods and inversion approaches. To do so, we must take into consideration and identify the optical components of the MRS. When passed through the instrument, special effects from the optical components will modify the observed object which will disturb the interpretation of the received data. The particularity of this work is that during the acquisition, we will encounter two major obstacles that will limit the diffraction of the observed object spatially and spectrally and must be taken into consideration during the process:

1. The optical response of the mirror that limit spatially the diffraction and changes according to the value of the wavelength.
2. The diffraction gratings response that limit spectrally the diffraction and also changes according to the value of the wavelength which will introduce a non-stationarity to our model.

In chapter 3, we will identify the MRS components and give the explicit and theoretical continuous formulas of the instrument, as for the chapter 4, we will develop an algorithm for the MRS model, apply it to a 3D cube made of two stars since we have not real data to test yet, as well as aboard the main problems of the MRS modeling listed in the previous paragraph and show the results of the algorithm.

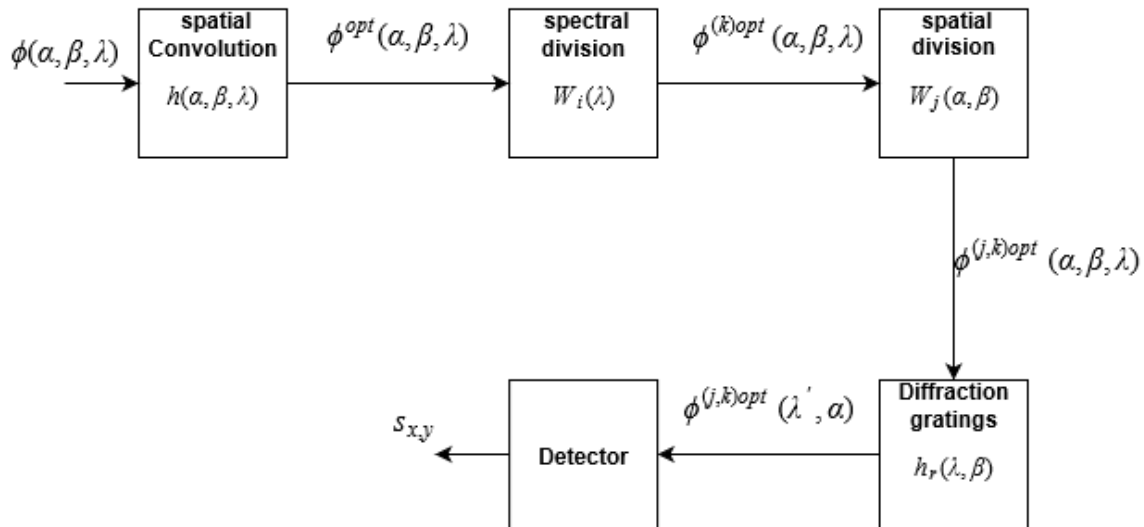
In chapter 5 we will use the direct model attributed to use linear inversion approaches in order to allow a better reconstruction and to obtain a 3D cube faithful as much as possible to the observed cube.

Direct model

3. MRS modeling

The JWST observes a 3D object $\phi(\alpha, \beta, \lambda)$ placed in the far field in the space. This object is composed of two spatial dimensions (α and β) and one spectral dimension (λ). Once observed, the collected object will go through some complex optical components of the MRS instrument. The resulting output received on the detector is a 2D image with one spatial dimension α and one spectral dimension λ which will depend also on the second spatial dimension β . The main purpose of this work is to be able to reconstruct the original 3D cube from the 2D received image. To do so, we must first identify these complex components of the MRS instrument by representing a block scheme of each optical component and find its explicit mathematical expression.

Figure 4: Block diagram representing the components of the MRS instrument



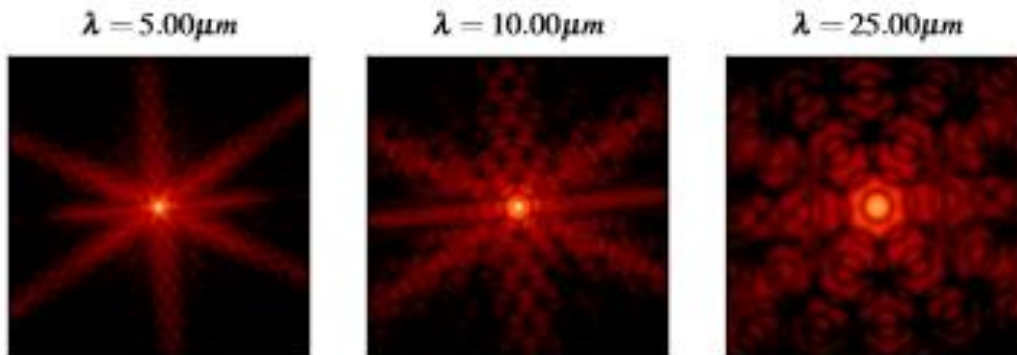
3.1. Spatial convolution

The optical system of the telescope will gather the light from the observed object and will diffract it to the focal plane where the telescope instruments are placed. The light is gathered in a parallel manner since the object is considered placed in the far field. As a result, the diffraction of the light is limited by a spatial 2D convolution with the optic response of the mirror known as the point spread function (PSF) and the observed object will be blurred. The particularity of this convolution is that the PSF vary along with the

wavelength of the 3D flux. More the wavelength is high more the telescope will be limited by the diffraction. The convolution can be written as [6]:

$$\phi^{opt}(\alpha, \beta, \lambda) = \int_{\alpha} \int_{\beta} \phi(\alpha', \beta', \lambda) h(\alpha' - \alpha, \beta' - \beta, \lambda) d\alpha' d\beta' \quad (3.1)$$

Figure 5: The PSFs below are obtained using the webbpsf simulator for the MIRI instrument in the JWST telescope for $\lambda = 5, 10$ and $15 \mu m$, we can clearly see that the PSF increase with the increase of the wavelength.

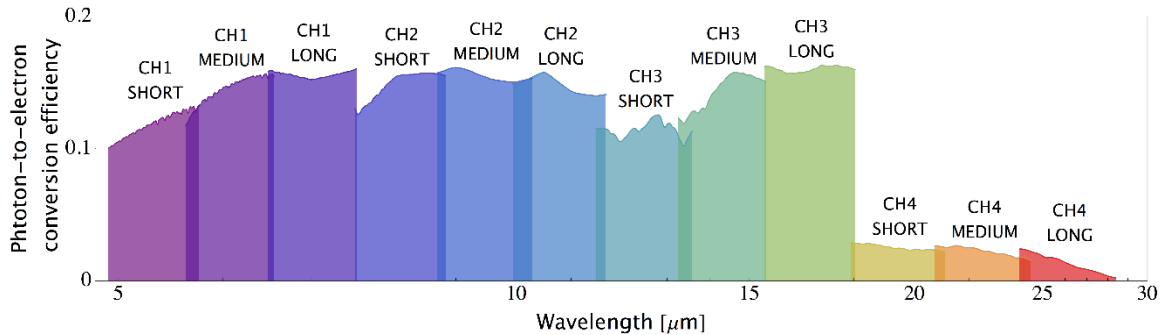


3.2. Spectral division

The MRS instrument will then observe the blurred object with a field of view up to $7.2''$ to $7.9''$ [1]. The full wavelength range in the MRS will be divided into four spectral channels using a simple pass-band separation by the dichroic filters. The four channels are seen simultaneously and every channel has its own wavelength coverage and its optimal resolution on the detector (*see table 1*). This method is adopted for the reason that we are not capable of measuring the whole spectra range at one time. Each exposure on the detector can only cover one third of the wavelength in each channel. To cover the whole range, we need three exposures, short (A), medium (B) and long (C) which leaves us with 12 spectral channels, each with its own field of view and wavelength coverage. The spectral division changes in function of the wavelength and can be written as:

$$\phi^{(k)opt}(\alpha, \beta, \lambda) = \phi^{opt}(\alpha, \beta, \lambda) \cdot W_k(\alpha, \beta, \lambda - \lambda_k) \quad (3.2)$$

Figure 6: A representation of the 12 spectral filters dividing the spectral channel into spectral channels (James Webb Space Telescope documentation)



3.3. Spatial division

Before the light in each channel go through the diffraction gratings, the object is spatially sliced and reformatted by the integral field unit (IFU). The blurred flux in every channel reaches its own image slicer which will decompose the image into several number of slices depending on the spectral channel. The IFU model has several advantages in the MRS instrument model [2]:

1. By dividing one spectral dimension into slice, it will be easier to eliminate a spatial dimension at the diffraction gratings since the observed flux is in 3D and the received image on the detector is in 2D. Ideally, the slice must be very thin but that will leave us with a null flux
2. The number of width changes between channels for the reason that the slice width is set to be less or equal to the FWHM of the PSF, and since the PSF changes according to the wavelength value, the number of width changes between channels, which will prevent the loss of light, a problem that we might have faced by using a long-slit model
3. . The IFU also permits to center the source in a narrow slit which can accelerate the acquisition procedure. The IFU align and format the segment onto the grating diffraction in a spectrograph.

Figure 7: A schematic representation on how the imaged is sliced in function of a spatial dimension and how the light from each slice is reformatted into an entrance slit spectrograph (Courtesy of Durham University)

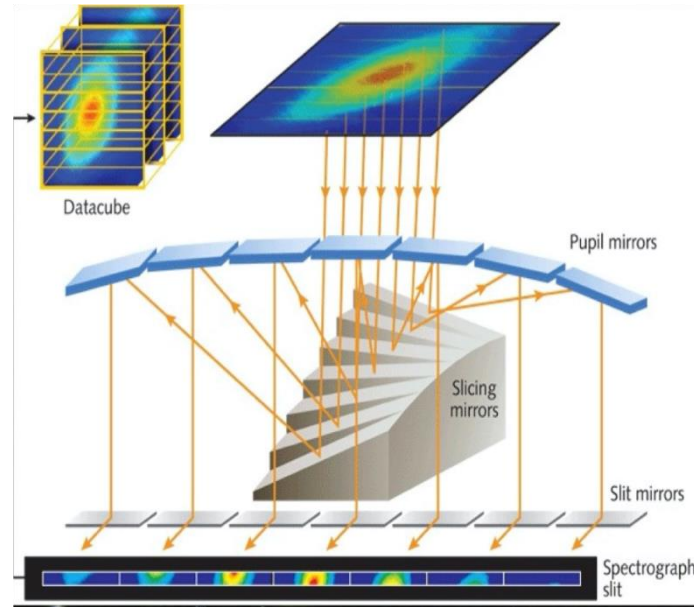


Figure 8: A representation of the 4 sliced channels observed simultaneously, each with its own FOV (James Webb Space Telescope documentation)

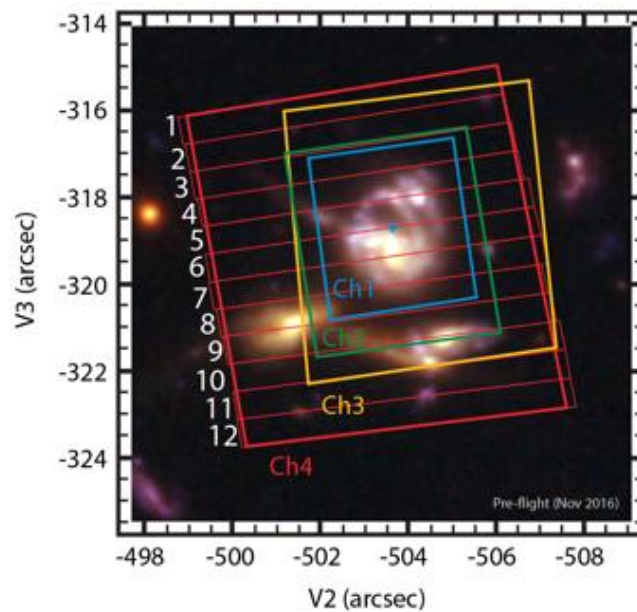


Table 1: Table showing the characteristics of the MRS IFU model: the wavelength coverage for each channel, FOV in arcsec, number and width of slices, pixel size on the detector and the spectral resolution (James Webb Space Telescope documentation)

Channel name with λ range	FOV (arcsec)	Number of slices	Slice width (arcsec)	Pixel size (arcsec)	Sub-band name	λ range	Spectral resolution $\lambda/\Delta\lambda$
Channel1 4.89-7.66	3.3x3.7	21	0.176	0.196	Short(A)	4.89-5.75	3320-3710
					Medium(B)	5.65-6.64	3190-3750
					Long(c)	6.52-7.66	3100-3610
Channel2 7.47-11.71	4.2x4.8	17	0.277	0.196	Short(A)	7.49-8.78	2990-3110
					Medium(B)	8.65-10.14	2750-3170
					Long(c)	9.99-11.71	2860-3300
Channel3 11.53-18.06	5.6x6.2	16	0.387	0.245	Short(A)	11.53-13.48	2530-2880
					Medium(B)	13.37-15.63	1790-2640
					Long(c)	15.44-18.05	1980-2790
Channel4 17.66-28.45	7.2x7.9	12	0.645	0.271	Short(A)	17.66-20.92	1460-1930
					Medium(B)	20.54-24.40	1680-1770
					Long(c)	23.95-28.45	1630-1330

3.4. Dithering

Dithering is a technique used by astrophysics that consists of moving the scene observed by a small amount and then re-observe. Dithering is adapted for many reasons, it helps with the artifacts detection because a given object is imaged on different parts of the detector, plus it allows a better reconstruction of lost information due to the spatial under sampling. The spatial division and dithering can be considered as spatial shifting and can be written as:

$$\phi^{(j,k)opt}(\alpha, \beta, \lambda) = \phi^{(k)opt}(\alpha, \beta, \lambda) \cdot W_j(\alpha - \alpha_j, \beta - \beta_j, \lambda) \quad (3.3)$$

3.5. Diffraction gratings

The light in each sliced reformatted and aligned by the slicer will be sent to the diffraction gratings where the light is dispersed into monochromatic lights depending on the wavelength. A lens is placed after the diffraction gratings to focalize each monochromatic light on the detector.

3.5.1. Diffraction impulse response

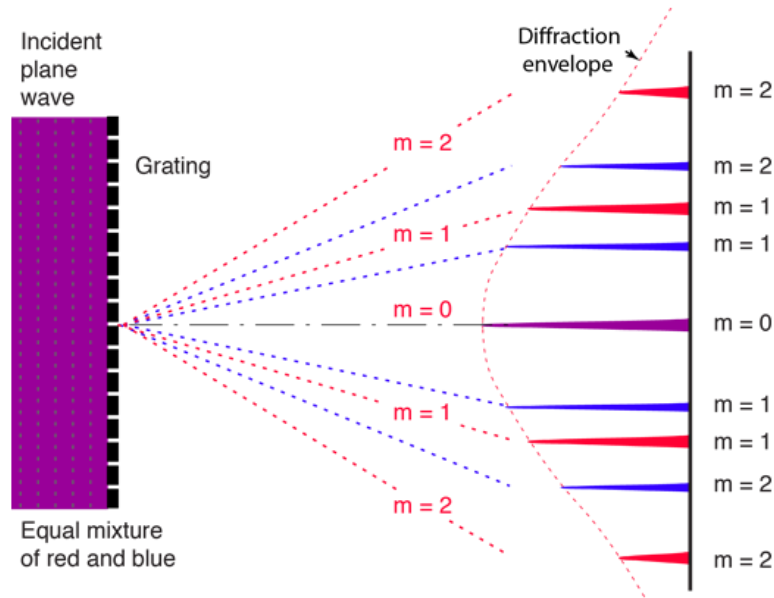
Consider a monochromatic light entering the diffraction gratings, the intensity response of the diffraction gratings for a monochromatic light will be approximated follow [4]:

$$h_r(\beta, \lambda', \lambda) \approx I_0 \text{sinc}^2\left(\frac{\pi b \lambda'}{\lambda}\right) \frac{\sin^2\left(N\pi a \sin\left(\frac{\lambda' - \beta - m}{\lambda} - \frac{m}{a}\right)\right)}{N^2 \sin^2\left(\pi a \sin\left(\frac{\lambda' - \beta - m}{\lambda} - \frac{m}{a}\right)\right)} \quad (3.4)$$

Where:

- I_0 represents the amplitude of the response.
- b represents the width of the gratings lens.
- N represents the number of gratings.
- a represents the step between the gratings
- $\text{sinc}^2\left(\frac{\pi b \lambda'}{\lambda}\right)$ represent the function that envelop the diffraction response.
- m represents the mode that we want to observe. For $m = 0$, the output does not move according to the wavelength. For that reason, we select the first mode, $m=1$ where the amplitude of the output is higher than the superior modes.

Figure 9: A representation of the grating and the diffraction process. The output of the grating can be seen in different modes. A purple light formed by a blue and red light enters the grating, for a mode $m=0$, we will not be able to observe the diffraction, however, for the mode $m = 1$ and $m = 2$ we can clearly see the diffraction of the light into red and blue. A diffraction envelope encounters the modes represented by $I_0 \text{sinc}^2\left(\frac{\pi b \lambda'}{\lambda}\right)$ in equation (3.4) (hyperphysics.phy-astr.gsu.edu)

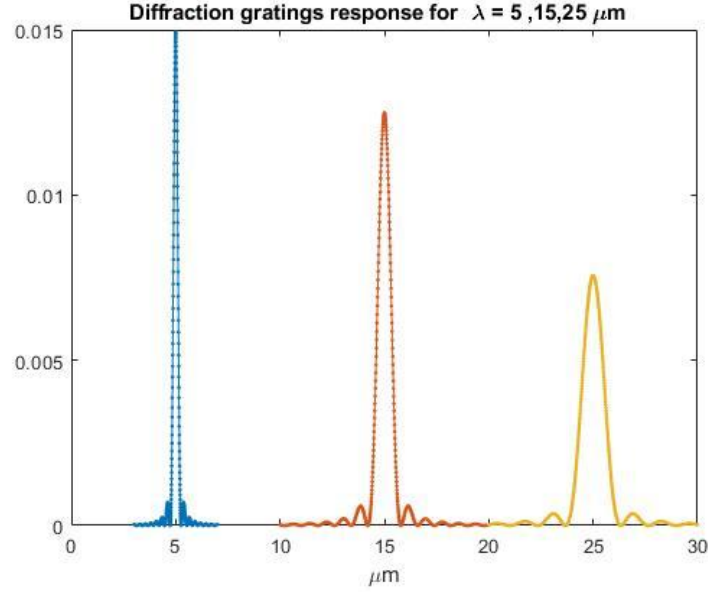


By applying the small angle approximation, $\sin^2\left(\pi a \sin\left(\frac{\lambda' - \beta}{\lambda}\right)\right)$ can be approximated as $\pi^2 a^2 \sin^2\left(\frac{\lambda' - \beta}{\lambda}\right)$ and by that, equation (3) can be written as follow:

$$h_r(\beta, \lambda', \lambda) \approx A \text{sinc}^2\left(N\pi a \sin\left(\frac{\lambda' - \beta}{\lambda} - \frac{m}{a}\right)\right) \quad (3.5)$$

In the ideal case, the output of the diffraction gratings for a monochromatic light is a perfect spectrum of Dirac that changes position on the spectral axis according to the wavelength value. In this report, the diffraction grating is not perfect, and will introduce a spectral blurring to the input. In equation (3.5), λ' is assimilated to λ but limited by the spectral PSF. The particularity of the PSF is that it changes while changing the wavelength value as shown in figure 10. The diffraction grating is a linear operator that produce non-stationary outputs and transforms the wavelength into a spatial position.

Figure 10: The diffraction gratings of a normalized response for 3 monochromatic light $\lambda = 5\mu\text{m}$, $15\mu\text{m}$ and $25\mu\text{m}$, we can clearly see that the impulse response increases with the increase of the wavelength value since h_r depends on λ .



3.5.2. Diffraction gratings output

For a linear and continuous input, the output of the diffraction gratings for a selected slit will be represented as follow:

$$\phi^{(i,j)opt}(\lambda', \alpha) = \iint_{\lambda, \beta} \phi^{(i,j)opt}(\alpha, \beta, \lambda) h_r(\beta, \lambda', \lambda) d\beta d\lambda \quad (3.6)$$

Equation (3.6) is represented by continuous sum depending on λ and β . This double integer will lead to a degeneration phenomenon where a couple of (λ, β) may lead to the same exit wavelength λ' , and that's also one of the reasons that led us to adopt the dithering method since by moving the telescope, the spatial dimension β is changed. Plus, the double integer allows the transition from a 3D object to a 2D object with one spatial dimension α and the output of the diffraction gratings that depends on the couple (β, λ) .

3.5.3. Diffraction gratings length calculations

Equation (3.4) depends on unknown parameters such as the length of the gratings represented by

$$L = N \times a \quad (3.7)$$

Where:

- N is the number of gratings.
- a is the step between the gratings.

Neither N or a are known, instead, we know the spectral resolution $\frac{\lambda}{\Delta\lambda}$ for every channel (see table 1). A proposed method to calculate L is adopted in this work, noting that we are not interested in calculating a which controls the position of the response since we will use in the following chapter an approximation of the gratings response that is independent of a . Finding L consist of following these steps:

1. Calculate the gratings PSF for a large number of L .
2. Determine the FWHM of the responses which means finding $\Delta\lambda$
3. Calculate the error between the known spectral resolution $\frac{\lambda}{\Delta\lambda}$ and the measured one

$$error_L = (exact - FWHM)^2 \quad (3.8)$$

4. Choose L as the minimizer of the error.

Table 2: A representation of the different values of the gratings length L for the different channels

Channels	Wavelength	L
Channel 1a	4.89-5.77	924
Channel 2a	5.65-6.64	895
Channel 3a	6.52-7.66	836
Channel 2a	7.49-8.78	813
Channel 2b	8.65-10.14	796
Channel 2c	9.99-11.71	763
Channel 3a	11.53-13.48	700
Channel 3b	13.37-15.63	556
Channel 3c	15.44-18.05	498
Channel 4a	17.66-20.92	474
Channel 4b	20.54-24.40	455
Channel 4c	23.95-28.45	400

3.6. Detector

The 2D flux coming out of the diffraction gratings will hit the detector. This photodetector is composed of a CCD matrix that creates electrons when photons are absorbed. This matrix contains square elements or pixels of size 1024x1024 where each pixel size is noted d . The resolution on the detector varies between channel and they are represented in arcsec in table 1. The detector can be modeled as a double integer of the received flux on the surface of the detector and can be expressed as follow:

$$s(x, y) = \int_{xd}^{x(d+1)} \int_{yd}^{y(d+1)} \phi^{(j,k)opt}(\lambda', \alpha) d\lambda' d\alpha \quad (3.9)$$

4. Simulation and results

The MRS model in the previous chapter was presented and explained in its continuous form. However, the detector receives a 2D data in its discrete form. Since the instrument model is very complex, it will be hard to obtain a discrete form of the instrument from the continuous form. In this chapter, we will consider that the sky observed is already in its discrete form having a resolution that we chose similar to the resolution of the detector (*see table 1*) plus, the components of the MRS instruments are also discrete. We chose to show simulations for the channel 2c of a 3D cube using MATLAB simulator.

4.1. Spatial convolution

The PSF is represented by a circulate matrix. In this case, the spatial convolution can be calculated using the Fourier transform and the PSF can be expressed as a diagonal matrix. The spatial convolution at every wavelength can be expressed as follow:

$$\phi_k^{\text{opt}} = F^t \Lambda_h F \phi_k \quad (4.1)$$

Figure 11: In the ideal case, the telescope observes a star in the space represented by a dot in the far field. figure (11) left represent the original 3D cube observed at $\lambda = 10.138 \mu\text{m}$ by the telescope. figure (11) right represent the cube at the same wavelength convoluted by the PSF

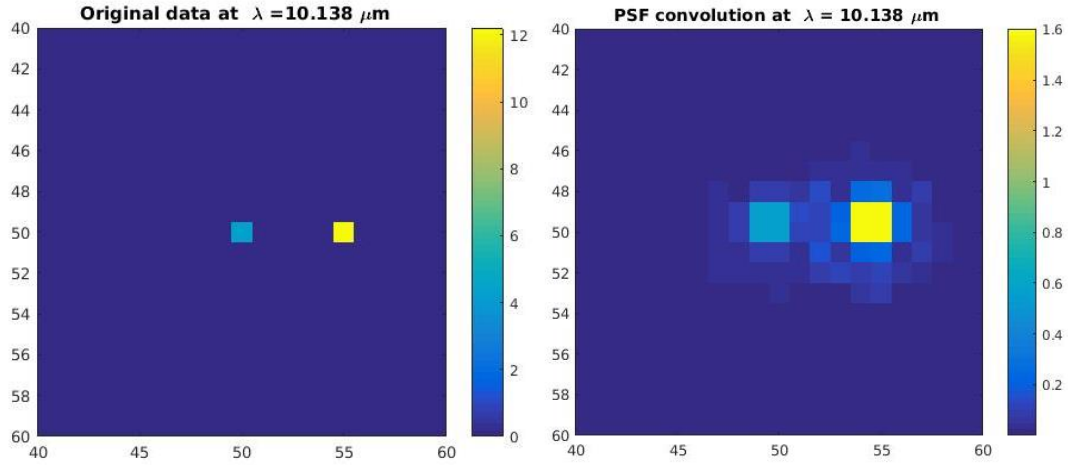
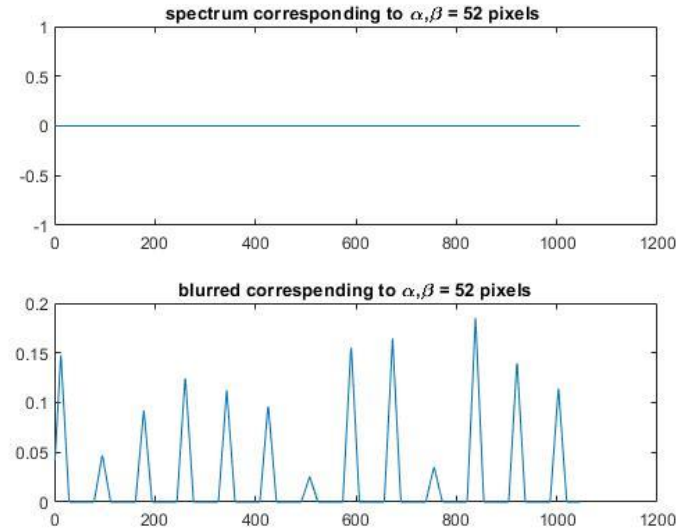


Figure 12: The spectrum axis for the original and blurred observed flux. We can clearly see that the blurring changes the observed object by blurring spatially the received cube



4.2. Cube spatial and spectral slicing

The spectral and spatial slicing consists of multiplying the observed cube limited by the diffraction with a matrix of selection let $[W_{j,k}]$ that slices the cube spectrally depending on the wavelength range desired to be observed and spatially depending on number of widths to be sliced in function of the spatial dimension β according to the chosen channel.

Figure 13: Representation of the IFU model that slices the image into 17 slices since in this report we are working on channel 2c (see table 1) at $\lambda = 10.138 \mu\text{m}$.

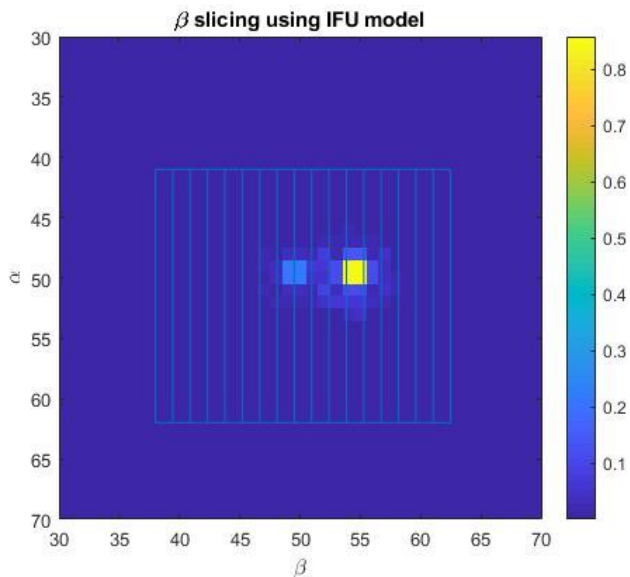
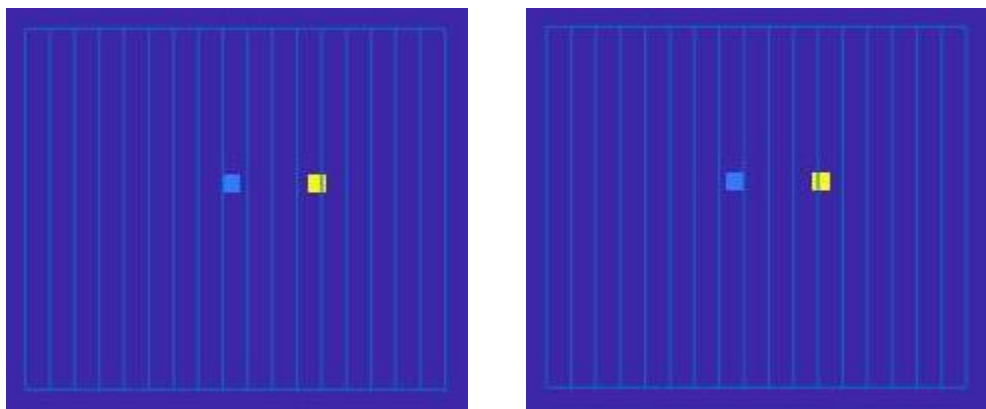


Figure 14: The figure on the right is a dithered version of the figure on the left at the same spatial coordination observed at the same wavelength values. The dithering is 0.196 arcsec which corresponds to 1 pixel on the detector.



4.3. Diffraction gratings

In this paragraph, we will discuss the output of the diffraction gratings for a given input and from the exact method we will explain an approximated method proposed by *Denis et Al*. Plus we will express the passage of the light in the diffraction gratings in its discrete form.

4.3.1. Diffraction gratings approximation

In the previous chapter, we have seen that the output of the diffraction gratings for a certain input depends on the spatial dimension β and on the spectral dimension λ . The output of the diffraction gratings in its discrete form for a single β is represented as follow:

$$s[\lambda'] = \sum_{\lambda} \phi^{(j,k)opt}[\lambda] \times h_r[\lambda, \lambda'] \quad (4.2)$$

Equation (4.2) represents the exact output of the gratings for any input. This method is proposed by *Rodet et Al* and it is feasible for every value on the spectral axis since it is easy to calculate the gratings response at any wavelength value and multiply it by the input value at the same wavelength. The complexity of this method appears when we want to sum the grating responses at different values of the wavelength. This complexity is due to the fact that we are summing a remarkable number of cardinal sinus.

An approached model was proposed by *Denis et AL* consists of calculating the non-stationary output of the gratings from the sum of stationary outputs using different versions of the weighted input. The use of the convolution in this approached method will simplify the complexity of the gratings output and will allow us to gain time by a factor of 5. This approximated method might add some unwanted information to the output of the gratings but in our point of view it has not such a great importance since the error between the two methods is low, plus, the diffraction grating response in equation (3.4) is already an approximated response.

The approached method is represented by the following equation [3]:

$$\sum_k (\phi^{(j,k)opt} \times w_k) * h_r^k \quad (4.3)$$

Applying this method consists of giving weights to every couple of pre-calculated response using equation (3.4) to obtain a collection of interpolated PSFs for the intermediate wavelength value of the couple.

The passage from the exact model to the approached model is calculated as follow:

- We consider in this demonstration that the exact pre-calculated responses are centered due to the fact that the approached model is the sum of the stationary weighted responses and we are not interested in their position. The approached diffraction response is the sum of two pre-calculated exact response h_r^0 and h_r^1 and can then be written as:

$$\hat{h}[\lambda, \lambda'] = h_r^0[\lambda'] + h_r^1[\lambda'] \quad (4.4)$$

- The non-stationary grating response is approximated by the sum of two stationary weighted grating responses. The output of the gratings for a monochromatic light at λ depends on the spatial resolution λ' so we shift h_r from λ' to its correct position at λ .

$$\hat{h}[\lambda, \lambda'] = h_r^0[\lambda - \lambda'] \times w_0[\lambda] + h_r^1[\lambda - \lambda'] \times w_1[\lambda] \quad (4.5)$$

- Replacing the non-stationary response by the approximated version in equation (4.2):

$$s[\lambda'] = \sum_{\lambda} \phi^{(j,k)opt}[\lambda] \times [h_r^0[\lambda - \lambda'] \times w_0[\lambda] + h_r^1[\lambda - \lambda'] \times w_1[\lambda]] \quad (4.6)$$

- Developing equation (4.6) in function of the sum in λ :

$$s[\lambda'] = \sum_{\lambda} \phi^{(j,k)opt} \times [\lambda] w_0[\lambda] \times h_r^0[\lambda - \lambda'] + \sum_{\lambda} \phi^{(j,k)opt}[\lambda] \times w_1[\lambda] \times h_r^1[\lambda - \lambda'] \quad (4.7)$$

- Writing (4.7) in its convolution form:

$$s[\lambda'] = \sum_k \sum_{\lambda} \phi^{(j,k)opt}[\lambda] \times w_k[\lambda] h_k[\lambda - \lambda'] \quad (4.8)$$

$$s[\lambda'] = \sum_k (\phi^{(j,k)opt} \times w_k) * h_r^k \quad (4.9)$$

- Summing the approached responses for every β value in the slice

$$s[\lambda'] = \sum_{\beta} \sum_k (\phi^{(j,k)opt} \times w_k) * h_r^k \quad (4.10)$$

Figure 15: A representation of the superposition of the exact and approached method for the channel 2c

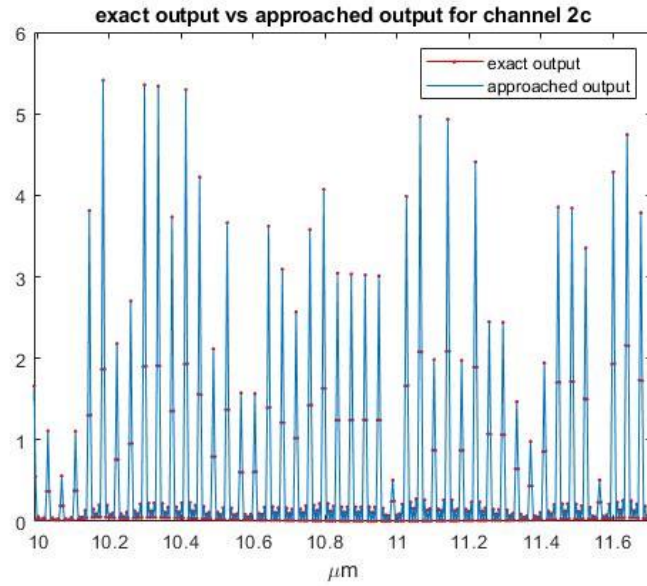
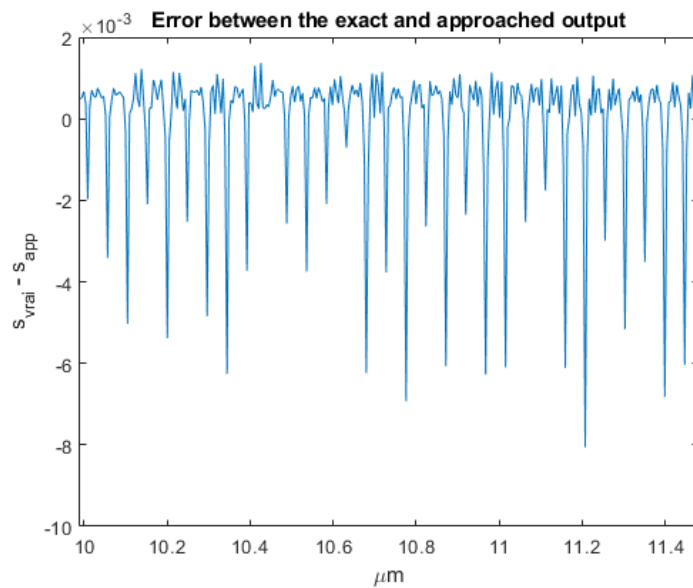


Figure 16: Error representation between the exact and approached method.



4.3.2. Diffraction gratings discrete calculation

As explained in the image slicing, the slice should not be very thin because it will set the observed flux to zero, meaning that the slice entering the cube depends on the spatial dimension β . Taking the 2D flux represented by the spatial dimension α and the spectral dimension λ on each value of β , each slice will undergo the following steps:

- Multiplication by the weight given from pre-calculated response on the left and on the right of the wavelength value desired to be calculated
- Convolution of each weighted input by its appropriate gratings response noted as h_r .
- Summation of the different versions of the convoluted weighted inputs.
- Summation the resulting 2D flux for each β value in the slice.

For a given beta, the explicit calculation of the gratings will be expressed as:

$$\begin{bmatrix} \mathbf{s}_1 \\ \vdots \\ \mathbf{s}_N \end{bmatrix} = [\mathbf{I}_1 \quad \dots \quad \mathbf{I}_k] \begin{bmatrix} \mathbf{C}_1 & \dots & \mathbf{0} \\ \vdots & \ddots & \vdots \\ \mathbf{0} & \dots & \mathbf{C}_k \end{bmatrix} \begin{bmatrix} \mathbf{W}_1 \\ \vdots \\ \mathbf{W}_k \end{bmatrix} \begin{bmatrix} \phi^{(j,k)opt}_1 \\ \vdots \\ \phi^{(j,k)opt}_N \end{bmatrix} \quad (4.11)$$

Where:

- $\phi^{(j,k)opt}$ represents the spectra for a fixed β value with a length of $N = 1024$ in our case.
- \mathbf{W}_k represents the weight matrix where k is the number of weighted versions that will multiply the input. For our calculation, $k = 2$ considering the weights given from the response on the left and right of the approached response. Each \mathbf{W} component in the vector is a matrix of size 1024×1024 in our case and is represented as follow:

$$\mathbf{W}_k = \begin{bmatrix} \mathbf{w}_1^k & \mathbf{0} & \dots & \mathbf{0} \\ \mathbf{0} & \ddots & \ddots & \vdots \\ \vdots & \ddots & \ddots & \mathbf{0} \\ \mathbf{0} & \dots & \mathbf{0} & \mathbf{w}_N^k \end{bmatrix} \quad (4.12)$$

- \mathbf{C}_k represents the gratings response appropriate to the weighted input. Each component in the matrix \mathbf{C} is a circulant matrix with a size of 1024×1024 . So, each component in the matrix \mathbf{C} are represented as a diagonal matrix.

Figure 17: The received 2D slice image shown on the detector with a white noise added. It is the output of the channel 2c slice 9. In this figure we can remarkably see the spectral dimension is spread on the detector in function of the spatial dimension

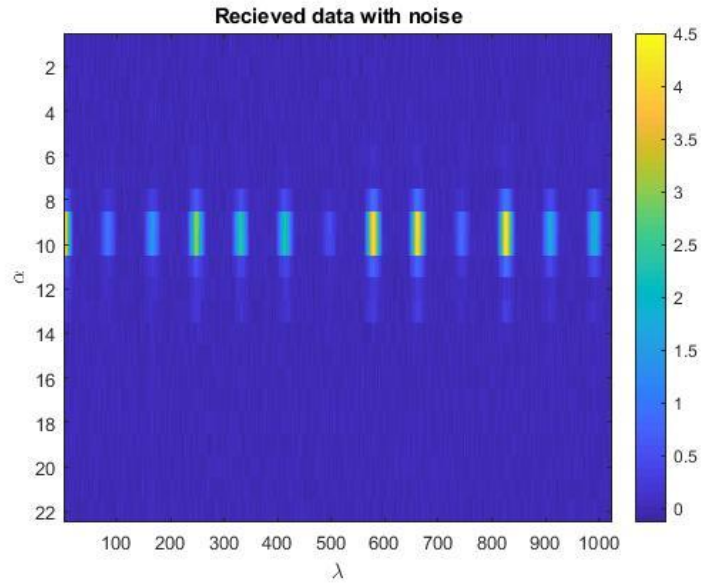
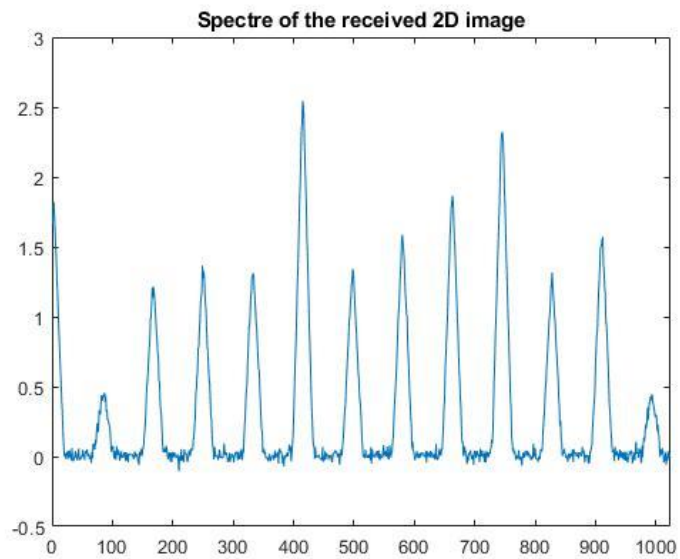


Figure 18: A representation the spectra of the received data with noise of channel 2c slice 9. We can see the effect of the gratings response on the spectra where we can see effects of the cardinal sinus on the image



Reconstruction and inversion methods

5. Reconstruction of the astrophysics cube

In the previous section, we have attributed a direct discrete model for the MRS instrument where all the operators that physically changes the observed object are linear and derivable. It was necessary to identify these operators in order to reconstruct the original 3D cube from a received 2D image shown on the detector, and use inversion approaches to enhance the reconstruction and inverse the effect of the spectral and spatial PSF on the object as well as the noise added through the channel. The direct linear model of the instrument is represented as follow:

$$s = Hx + n \quad (5.1)$$

Where:

- s is the received 2D image
- H represents the operator that the observed object will undergo before hitting the detector
- x is the original observed cube represented as $\phi(\alpha, \beta, \lambda)$ in the previous chapter
- n the white noise added through the channel.

5.1. Least squares method

Since the components of the MRS are linear and derivable, we can say that the operator H is linear and derivable and as a result we chose the least square method to inverse our received image.

- The least square criterion is represented as:

$$J_{ls}(x) = \|s - Hx\|^2 \quad (5.2)$$

- By developing the criterion, we obtain:

$$J_{ls}(x) = (s - Hx)^t (s - Hx) \quad (5.3)$$

$$J_{ls}(x) = x^t H^t H x - 2s^t H x + s^t s \quad (5.4)$$

- By nullifying the calculated gradient of J_{ls} we calculate the minimizer represented as:

$$\hat{x}_{ls} = (H^t H)^{-1} H^t s \quad (5.5)$$

5.2. Ill-posed problem and regularization

The operator H in equation (5.5) is not stable, meaning that a small variation in the values of the received image can lead to a noise explosion in the reconstructed cube. To avoid noise explosion, we must add a penalty to the equation to regulate the operator H .

- The penalized criterion is the represented as:

$$J_{PLS}(x) = \|s - Hx\|^2 + \mu \|Dx\|^2 \quad (5.6)$$

$$J_{PLS}(x) = x^t H^t H x - 2s^t H x + s^t s + \mu D^t D x \quad (5.7)$$

- By nullifying the calculated gradient of J_{pls} , the penalized minimizer is represented as:

$$\hat{x}_{pls} = (H^t H + \mu D^t D)^{-1} H^t s \quad (5.8)$$

5.3. Simulation and results

We have attributed a direct model for the MRS model noted H in equation (5.1), in order to apply the inversion approach, we must find the transpose of each component in the MRS instruments to find H^t as well as the optimal value of the regularization term μ .

5.3.1. Transpose calculation

We will give an explicit theoretical form of the transpose discrete direct model for one slice in the detector. For a whole cube reconstruction, we make the same calculations for each slice at every channel.

The transpose model of the direct model is applied following the next steps:

1. Each 2D slice is transform to a 3D slice with the exact number of β as the slicing in the previous chapter
2. For each β value in the slice we create 2 exact versions of the data. Every approached weighted response is convoluted by the left pre-calculated response from equation (3.4) and multiply it by the its appropriate weight. We do the same for the second version with the right pre-calculated response.
3. We sum both versions for each β .

The first three steps can be resumed as follow:

$$[x_1 \quad \dots \quad x_n] = [W_1 \quad \dots \quad W_k] \begin{bmatrix} C_1^t & \dots & \mathbf{0} \\ \vdots & \ddots & \vdots \\ \mathbf{0} & \dots & C_k^t \end{bmatrix} \begin{bmatrix} I_1 \\ \vdots \\ I_k \end{bmatrix} \begin{bmatrix} s_1 \\ \vdots \\ s_n \end{bmatrix} \quad (5.9)$$

- Each matrix C_k is a circulate Toeplitz matrix that can be diagonalized in Fourier

4. The transpose output of the diffraction gratings is the multiplied by the transpose of the selection matrix in paragraph 4.2, represented as $[W_{j,k}]^t$
5. Calculate the transpose of equation (4.1), since the optic PSF is a circulate matrix, we compute the PSF through FFT diagonalization. The transpose of the spatial optic response is represented as follow:

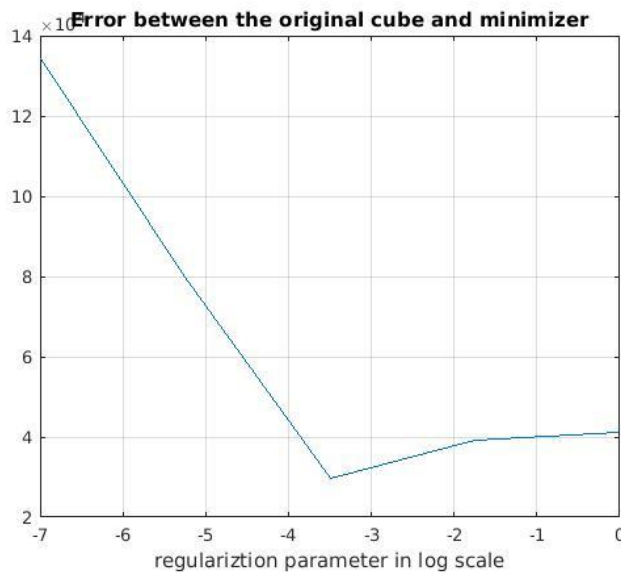
$$\hat{x} = F^t \Lambda_h^+ F x \quad (5.10)$$

5.3.2. Calculate optimal μ

μ represents the regularization term, for a very low μ , the reconstructed image will be very edgy, as for a high μ , the reconstructed image will be smoothed. We must find the optimal regularization term to apply it in equation (5.9). A proposed method is to find the error between the original cube and the reconstructed cube for different value of μ and keep the μ corresponding to the minimum error. The error is calculated by using the following formula:

$$\sum_{\alpha} \sum_{\beta} \sum_{\lambda} (x(\alpha, \beta, \lambda) - \hat{x}(\alpha, \beta, \lambda))^2 \quad (5.11)$$

Figure 19: A graph representing the error between the minimizer and the original cube, for $\mu = 10^{-3.5}$ we can have the minimum error between the two cubes.



5.3.3. Optimization algorithm

It is very complex to calculate the minimizer in equation (5.9) since $(H^t H + \mu D^t D)^{-1}$ is very complicated to calculate. However, optimization algorithms are used to solve iteratively a complex system of linear equations. The gradient calculated in equation (5.9) can be written in its linear form:

$$\nabla J_{pls}(\hat{x}) = A\hat{x} - b = 0 \quad (5.12)$$

Where:

- $A = H^t H + \mu D^t D$
- $b = H^t s$

The same \hat{x} used to minimize the $J_{pls}(x)$ is also the solution for the linear equation $Ax = b$. The minimizer is known to be unique since $J_{pls}(x)$ is convex.

After writing the quadratic function to its equivalent in equation (5.13), we will adopt the gradient conjugate strategy to solve the optimization problem where the iteration is represented as:

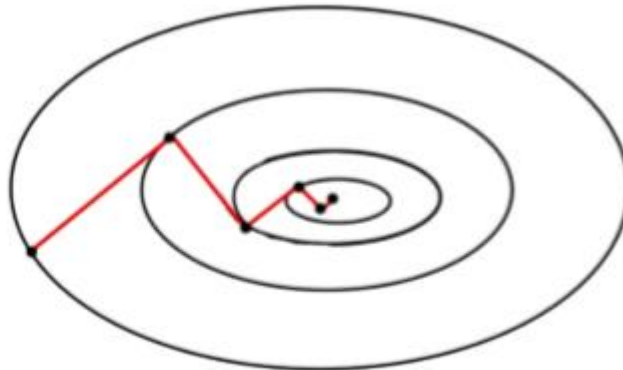
$$x_{k+1} = x_k + \alpha_k p_k \tag{5.13}$$

Where:

- p_k is the search direction for each iteration k
- α_k is the step length for each iteration k .

The method consists of starting from a chosen position x_0 and then step walk in a linear convergent form towards the solution by computing the direction and the step length for every iteration (*see annex1*)

Figure 20: A representation of the convergence of the solution using the gradient conjugate(<https://doi.org>)



5.3.4. Results

Figure 21: A reconstructed cube without inverting the effect of the spatial and spectral PSFs and the white noise. We can still see the effect of the convolution near the stars that adds unwanted information.

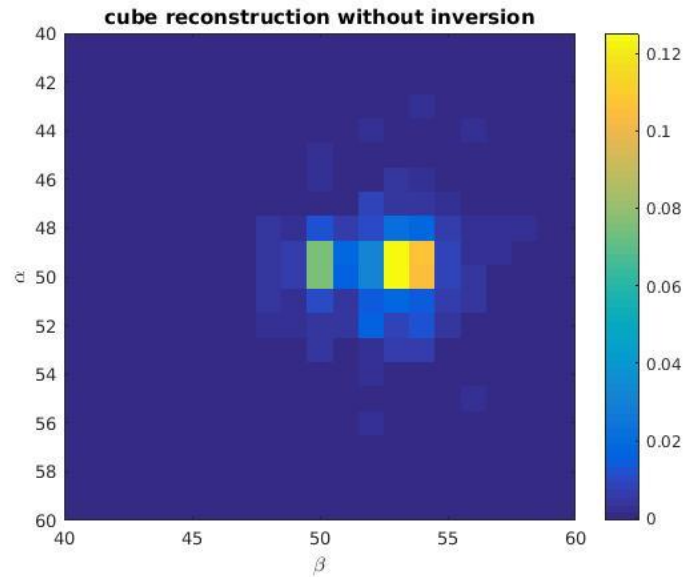


Figure 22: A reconstructed cube with the optimal $\mu = 3.1623e-4$. In this image we can see a major role of the artifacts, and that's a problem encountered when using the least square methods

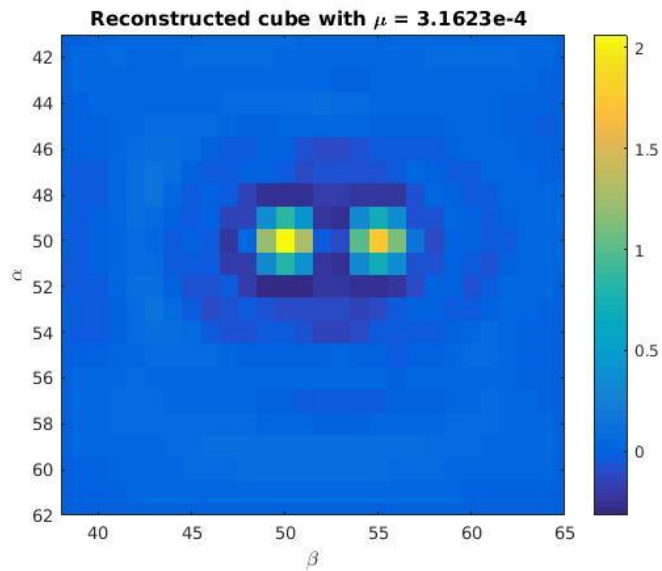


Figure 23: Two plots representing the spatial dimension β for $\alpha = 50$ pixels and $\lambda = 100 \mu\text{m}$. The first plot corresponds to the original cube and the second plot corresponds to the minimizer

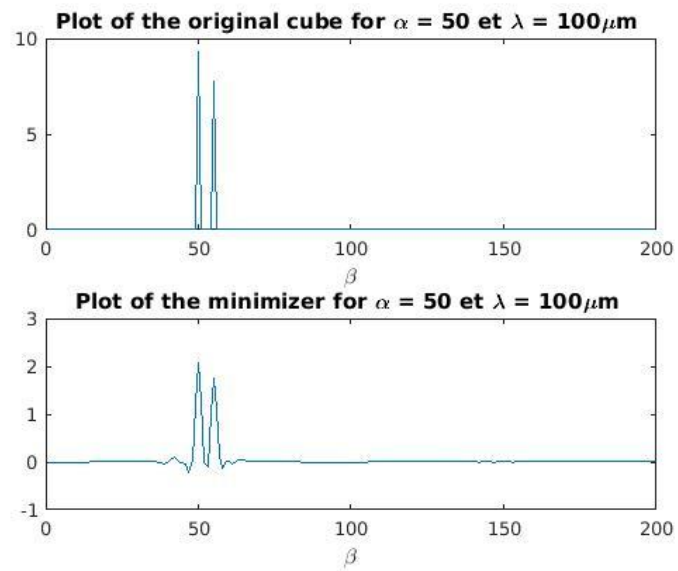


Figure 24: Two plots representing the spatial dimension β for $\alpha = 50$ pixels and $\lambda = 100 \mu\text{m}$. The first plot corresponds to the blurred cube and the second plot corresponds to the minimizer. We can clearly notice that the minimizer has inverted the spatial convolution effect

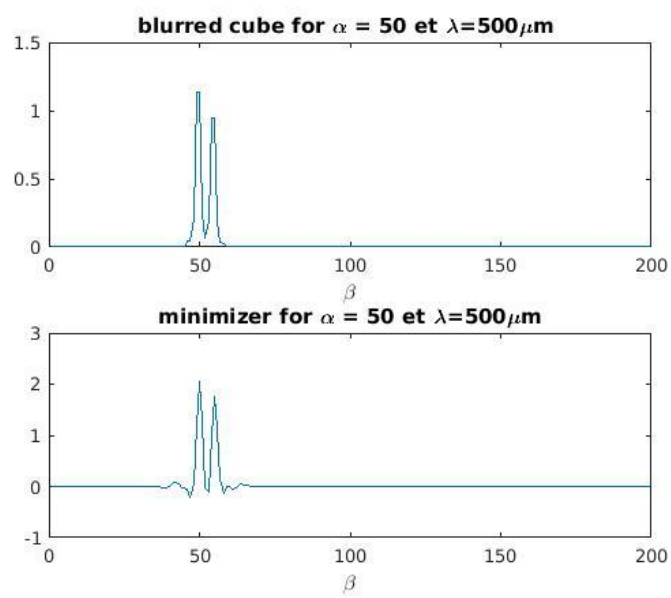
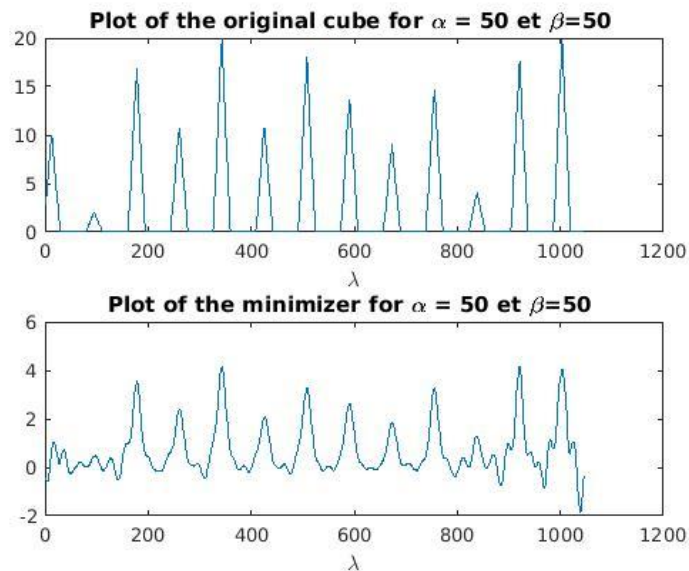


Figure 25: A representation of the spectral axis for α and $\beta = 50$ pixels. We notice that at the end, the specter of the reconstructed cube has weird effects, that comes from the fact that we used FFT computation that considers the operator H is circulate, but in the matter of fact, the operator is not circulant which causes these artifacts at the 2 extreme sides of the spectral axis



Conclusion and perspective

6. Conclusion

In this report, we studied each optical component of the MRS instrument, and gave the explicit mathematical formula for each of them in order to obtain a direct model that is faithful to the real simulator. We then discretized each of the components to be able to write and simulate of the MRS model using MATLAB simulator.

The last part of the report was contributed to the reconstruction of the original cube using inversion approaches, and showed simulations and cube reconstruction for one channel. The least square method might not be the perfect solution for the reconstruction in our case. Another solution will be proposed in the continuity of this internship.

The originality of this work was the use of the approached PSF model proposed by *Denis et Al* and apply it in our study at the diffraction gratings where its PSF introduce a non-stationarity to the model.

7. Perspectives

In this work, we built an algorithm that is capable to reconstruct the original data for only one channel, plus we used a simple reconstruction method that produces artifacts and not very optimal. In the future work, we will work on the reconstruction of a whole cube for all the channel with more practical astrophysics data.

The direct model of the MRS instrument will be used in the future to be merged with the direct model of the imager (MIRIM) of the MIRI instrument developed by the PHD student HADJ-YOUSSEF Amin. The main reason behind this fusion is due to the fact that the MRS have a limited spatial resolution but a view but a high spectral resolution, as for the imager, it has a high spatial resolution but a limited spectral resolution, and our purpose is to build a simulator that is capable to work on hyper resolution for spatial and spectral measures. Many problems will be encountered specially the heterogeneity of the filters of both instruments, plus the blurring that will be always present by the PSF.

This merged direct model will be used to reconstruct the 3D cube. The reconstructing method will mainly be consisting of these following steps:

1. Estimate \hat{x} from the MRS model
2. Estimate the specter noted s_i from \hat{x} using the source separation method
3. Re-estimate \hat{x} and s_i using the merged model of the two instruments (*Boucas-Dias*)

I. Annex 1

The gradient conjugate method is based on the A-conjugate direction model where a set of vectors $\{p_0 \dots p_{n-1}\}$ are conjugate with respect to the matrix A as $p_{k-1}^t A p_k$.

This method is an iterative method that converges towards the solution following these steps:

- Choose initial position x_0
- Calculate the initial residual $r_0 = Ax_0 - b$
- Calculate the first step direction $p_0 = -r_0$
- Compute the step length $\alpha_k = \frac{r_k^t r_k}{p_k^t A p_k}$ where k is the iteration number noting that in this method all the iterations have the same step size.
- Having p_0 and α_0 we can compute the first iteration $x_1 = x_0 + \alpha_0 p_0$
- The residual for the following iteration is $r_{k+1} = r_k + \alpha_k A p_k$
- The new step method is expressed as $p_k = -r_k + \beta_k p_{k-1}$ where β_k impose the condition of $p_{k-1}^t A p_k$ and expressed as $\beta_k = \frac{r_{k+1}^t r_{k+1}}{r_k^t r_k}$
- The next step direction is calculated as: $p_{k+1} = -r_{k+1} + \beta_k p_k$
- We can finally calculate the iterative solution $x_{k+1} = x_k + \alpha_k p_k$

References

- [1] <https://jwst-docs.stsci.edu/display/JTI/MIRI+Medium-Resolution+Spectroscopy>
- [2] Wells, M., Pel, J.-W., Glasse, A., Wright, G. S., Aitink-Kroes, G., Azzollini, R., ... Wright, D. (2015). The Mid-Infrared Instrument for the James Webb Space Telescope, VI: The Medium Resolution Spectrometer, 1–49. <https://doi.org/10.1086/682281>
- [3] Denis, L., Thiébaud, E., Soulez, F., Becker, J.-M., and Mourya, R., “Fast approximations of shift-variant blur,” *International Journal of Computer Vision* 115(3), 253–278 (2015).
- [4] Etude des réseaux de diffraction (PC*). (n.d.).
- [5] <https://www.jwst.nasa.gov/>
- [6] Hadj-Youcef, M. A., Orioux, F., Fraysse, A., & Abergel, A. (2017). Restoration from multispectral blurred data with non-stationary instrument response. *25th European Signal Processing Conference, EUSIPCO 2017, 2017–January*, 503–507. <https://doi.org/10.23919/EUSIPCO.2017.8081258>
- [7] Refsn, R. H. (2009). a Brief Introduction To the, *1*, 9–11. <https://doi.org/10.1016/B978-0-12-801529-2/00001-5>
- [8] Jérôme Idier, editor. *Approche bayésienne pour les problèmes inverses. Traité IC2, Série traitement du signal et de l’image*, Hermès, Paris, 2001.